Calibration, alignment and tracking performance of the CMS Silicon Strip Tracker

Martin Weber on behalf of the CMS collaboration

Institut für Experimentalphysik, Universität Hamburg, Germany

Abstract

After its installation in the CMS experiment, the CMS silicon tracker has been commissioned, calibrated and aligned based on several million reconstructed tracks, recorded during extended cosmic ray data-taking in 2008 and 2009. The collision data at 900 GeV and 2.36 TeV which were recorded by the CMS experiment in December 2009 allowed to repeat the calibration measurements and derive compatible results. Calibration results are shown for the silicon strip detector only, whereas alignment and tracking performance are given for the complete CMS tracker, including the silicon pixel system.

Key words: silicon detectors, calibration, Lorentz angle, tracking, alignment
PACS: 06.60.Sx, 07.05.Kf, 29.40.Gx, 29.40.Wk

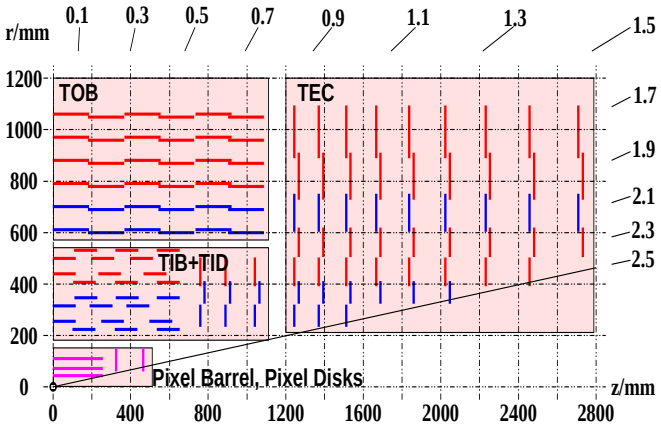

Figure 1: *r*-*z* view of one quarter of the CMS tracker.

1. The CMS Tracker

The main components of the CMS experiment at the CERN LHC are a precise muon spectrometer, a sampling brass hadron calorimeter, an electromagnetic lead-tungstate crystal-calorimeter, a superconducting coil that provides a nominal solenoidal 3.8 T magnetic field, a silicon strip and pixel tracker, and a two-stage triggering system. It is described in detail in Reference [1].

Fig. 1 shows an *r*-*z* view of the modules in one quarter of the CMS tracker. The pixel detector comprises three barrel layers and four forward disks, two on each side of the barrel, made up of 1 440 modules with n-on-n silicon sensors and a pixel size of 100 µm($r\phi$) × 150 µm(z). The strip detector consists of four subsystems and employs 320 µm (thin) and 500 µm (thick) sensors built from industrial 6" wafers in p-on-n technology. Modules in the four layers of the Tracker Inner Barrel (TIB), in the three disks of the Tracker Inner Disk (TID), and at $r < 60$ cm in the nine disks of the two Tracker Endcaps (TEC) contain one thin sensor. Modules in the six layers of the Tracker Outer Barrel (TOB), and at $r > 60$ cm in the TEC contain two daisy-chained thick sensors. In total, the strip tracker contains 15 148 modules with a strip pitch ranging from 80 µm to 205 µm. On the modules, four or six APV25 [2] readout-ASICS are mounted, each serving 128 channels. The analog readout chips amplify, shape and store the detector signals and forward them on a trigger request via linear laser-drivers and optical fibres to the front-end drivers (FEDs), where they are digitized.

2. Data and Monte-Carlo samples

During 23 days in October and November 2008, the CMS experiment recorded 270 million cosmic ray triggered events at its nominal magnetic field of 3.8 T. This data taking period is also known as Cosmic Run at Four Tesla (CRAFT). A fraction of about 10% of the events contained tracks passing the CMS tracker and were used for alignment and calibration purposes. About 21 million simulated cosmic muon events were used for comparison.

In December 2009, CMS recorded collision data of about 10 μb^{-1} of integrated luminosity at 900 GeV proton-proton center-of-mass energy and about 400 mb^{-1} at 2.36 TeV. Simulated collision data were used for comparison purposes.

3. Commissioning

The strip tracker commissioning procedure, detailed in Reference [3], consists of identifying responsive devices, establishing a cable map, relative synchronization of the readout electronics, adjusting the readout system gain and fine-tuning the on-detector readout electronics. After this procedure, about 98.6% of the strip tracker modules were found to be functional.

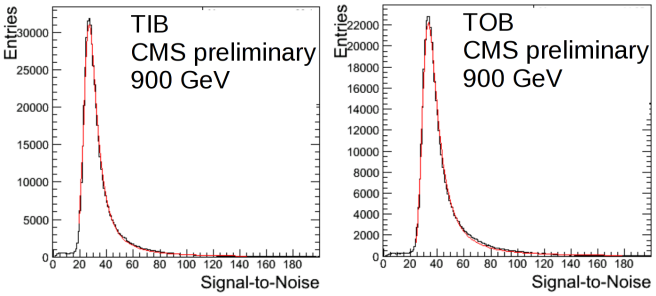

Figure 2: Signal-to-noise ratio in TIB and TOB during 900 GeV collisions.

4. Calibration

After measuring the noise and, following a synchronization to particles, measuring the signal-over-noise ratio, the Lorentz angle is measured and an absolute calibration of the energy scale is performed.

4.1. Signal and noise

The noise of the silicon detector and readout electronics is measured using a random, low-frequency trigger (~10 Hz) in the absence of signal with the APV operating in peak mode. After the subtraction of a common, synchronous variation of all 128 channels of the APV under consideration, the noise is measured for each strip as the standard deviation of the randomly fluctuating signal arriving at the front-end drivers. As the silicon detector noise depends on the strip capacitance and thus on the (effective) strip length, the noise in all different modules has been measured and, requiring a linear dependence on the strip length, the following parameterization is found from CRAFT measurements:

$$\text{noise}(e^-) = (427 \pm 39) + (38.7 \pm 3.0) \times \text{length(cm)} \qquad (1)$$

The signal-to-noise ratio is a benchmark for the tracker performance. Traversing particles deposit charge in one or more adjacent strips. Cluster signal $s = \sum_i s_i$ and cluster noise $n = \sqrt{\sum_i n_i^2}/n$ are defined by the contributions of the individual $i = 1 \ldots n$ strips with strip signal s_i and strip noise n_i. Figure 2 shows the signal-to-noise ratio as determined during 900 GeV collisions for both TIB and TOB modules.

Although sensors in TOB are 500 µm thick and thus collect approximately 50% more charge than sensors in TIB with 320 µm thickness, the increased capacitance of the two daisy-chained sensors in TOB results in an only slightly larger signal-to-noise ratio of 32.6 compared to 26 in TIB, where both values are large enough to allow an efficient identification of particles with negligible background.

4.2. Lorentz angle

Since in both TIB and TOB the electric and magnetic field in the sensors are orthogonal to each other, electrons drift with a Lorentz angle θ_L relative to the electric field direction, affecting the cluster size. If the track direction, projected on the plane perpendicular to the strips, is collinear with the drift direction, a minimum cluster size is found. Figure 3 shows the cluster size as a function of the track angle θ_t for TOB layer 4. By fitting a function $f(\theta_t) = p_0|\tan(\theta_t) - p_1| + p_2$ with parameters p_i to the data taken during CRAFT, the Lorentz angle can be extracted from $p_1 = \tan(\theta_L)$. Values of $\tan(\theta_L) = 0.07 \pm 0.02$ and $\tan(\theta_L) = 0.09 \pm 0.01$ are found for TIB and TOB, respectively.

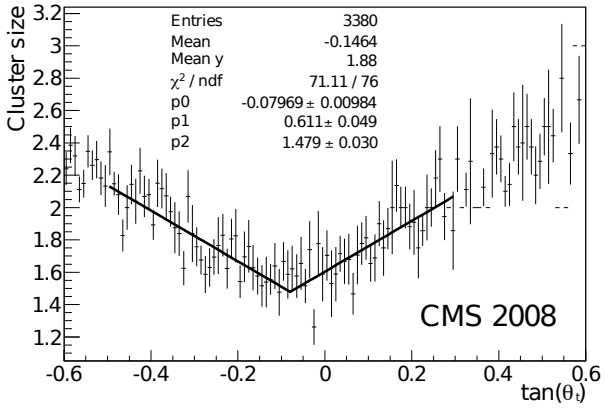

Figure 3: Measurement of the Lorentz angle in TOB layer 4.

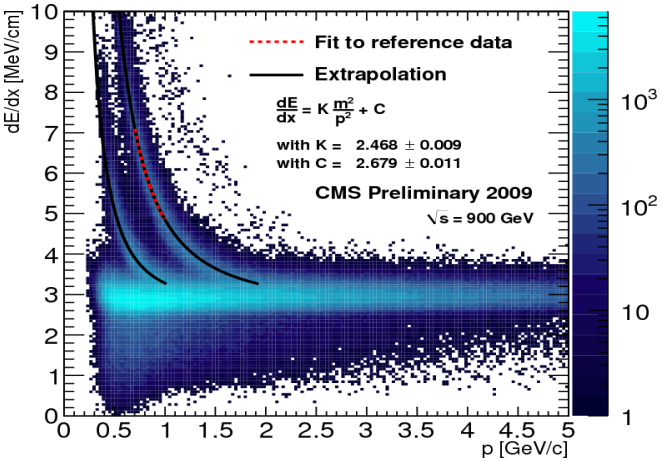

Figure 4: dE/dx of particles produced during collisions at 900 GeV.

4.3. Energy calibration

Energy calibration aims at establishing a conversion ratio from the signal values digitized in the front-end drivers to the number of electron-hole pairs generated by the traversing particle in the silicon sensor, thus enabling particle identification by energy loss measurements. This conversion factor depends on the silicon sensor properties and depletion voltage and various settings of the electronic and optic transmission lines. Therefore the calibration procedure consists of several consecutive steps, fully described in Reference [3].

Cosmic muons are used to establish the absolute calibration. Since the muons on average leave the same signal per unit length in each sensor, the most probable values of the Landau-distributions are used offline as correction factors per APV and thus uniformity is ensured. However, this does not set the ab-

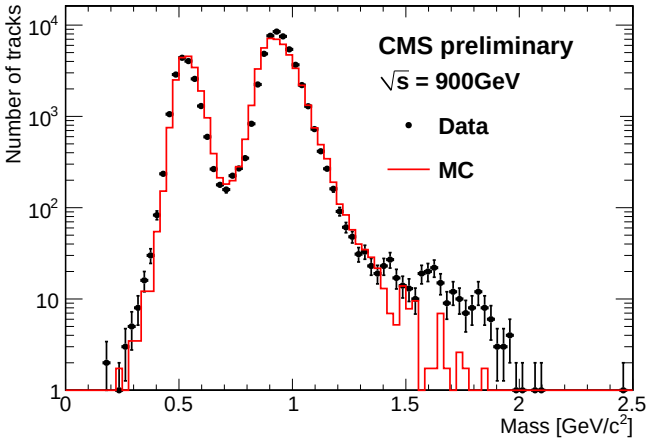

Figure 5: Mass extracted from energy measurements after requiring $dE/dx >$ 4.15 MeV/cm, for both collision data at 900 GeV and Monte-Carlo.

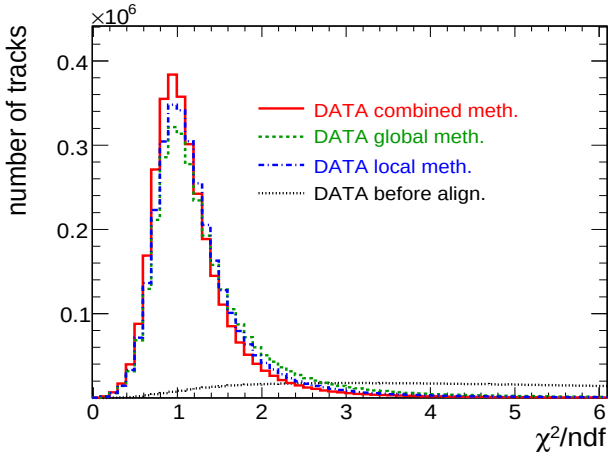

Figure 6: Distribution of χ^2/ndf before and after alignment.

solute scale. Therefore, in a last step, the absolute calibration scale is established by fitting the Landau-Vavilov-Bichsel function of the most probable energy loss per unit length Δ_p/x as a function of the muon momentum. In order to increase statistics, signals from all sensors of a certain type were added together, which is possible after uniformity is achieved.

The calibration constants obtained during CRAFT have consequently been applied to collision data. Figure 4 shows the dE/dx distribution of particles crossing the silicon sensors versus measured momentum, together with expectations for kaons and protons. Once a cut of $dE/dx > 4.15$ MeV/cm is applied, the mass information can be extracted from the dE/dx measurement. Figure 5 shows this mass distribution and shows a clear separation of kaons from protons. A good agreement of data and Monte-Carlo prediction is observed.

4.4. Hit efficiency

The hit finding efficiency has been determined for each barrel layer after aligning the tracker as described in section 6. Tracks are reconstructed as described in section 5 and refitted excluding the hits (if any) in the layer under consideration. The hit efficiency then is evaluated by measuring the number of times a hit is found on those sensors the track is penetrating in the given layer. An efficiency of >90% is found for all layers. When known problems are excluded, the efficiency exceeds 98.5% in all layers.

5. Track reconstruction

The standard track reconstruction algorithm for collisions, the "Combinatorial Track Finder" (CTF) [4] can be run in either cosmic muon or collision reconstruction mode. Tracks in cosmic muon mode are reconstructed from seeds found in the outer tracker layers and hits are added proceeding to the inner layers. In collision mode, seeds are searched first in innermost layers and hits are added proceeding outwards. The track reconstruction efficiency for both modes has been evaluated on cosmic muon data. Firstly, the efficiency of the cosmic muon reconstruction mode is determined. Using muon system data only, events are selected where a track in the top and bottom of the muon system has been reconstructed and passes through the inner detector. In these events the reconstruction efficiency for the CTF algorithm exceeds 99.7%. Secondly, the performance of the CTF collision mode is evaluated. To this end, events containing tracks passing through all three layers of the pixel system are selected. In these events, one reconstructed track leg is used as a reference track and a second track leg determines the efficiency, which is measured to be 98.9%, compatible with Monte-Carlo simulations within 1%.

6. Alignment

6.1. Method

Alignment, i. e. determining position and orientation of all silicon pixel and strip sensors, is performed by minimizing the objective function

$$\chi^2(p,q) = \sum_{i}^{tracks} \sum_{j}^{hits} r_{ij}^T V_{ij}^{-1} r_{ij} \qquad (2)$$

with respect to alignment parameters p and track parameters q_j, where r_{ij} are the track residuals and V_{ij} their covariance matrix. About 3.2 million cosmic muon tracks have been used in a multi-step alignment procedure [5]. Two alignment algorithms are consecutively applied to the data: A global method (Millepede II) and a local method (HIP), each performing a full alignment in several steps.

6.2. Results

Figure 6 shows the distribution of χ^2/ndf which qualitatively shows similar behaviour as the minimized quantity (2), before alignment and after alignment with the global, local and combined method. A clear improvement after alignment is observed. This improvement is also observed in the hit residuals, i. e. the difference between track extrapolation on the sensor surface and measured hit in all subdetectors. However, after alignment, the residual width contains not only contributions from remaining misalignment or systematic effects, but

	before [μm]	combined [μm]	combined MC [μm]	ideal MC [μm]
BPIX (u')	328.7	2.6	2.1	2.1
BPIX (v')	274.1	4.0	2.5	2.4
FPIX (u')	389.0	13.1	12.0	9.4
FPIX (v')	385.8	13.9	11.6	9.3
TIB (u')	712.2	2.5	1.2	1.1
TOB (u')	168.6	2.6	1.4	1.1
TID (u')	295.0	3.3	2.4	1.6
TEC (u')	216.9	7.4	4.6	2.5

Table 1: RMS of the distribution of $\mu_{1/2}$ for modules with more than 30 hits before and after combined alignment compared to Monte-Carlo alignment and ideal Monte-Carlo.

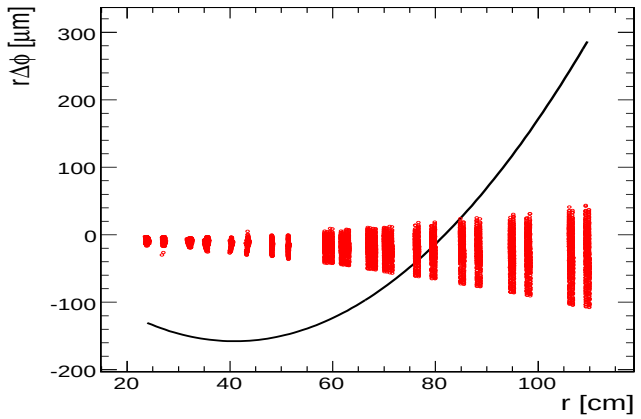

Figure 7: Relative shift $r\Delta\phi$ of modules as a function of r for a layer rotation (parabolic line, black) and after alignment (vertical bands, red).

also from random hit, track extrapolation and multiple scattering uncertainties. Therefore, as a measure of alignment quality, for each module the median of the residual $\mu_{1/2}$ is computed and histogrammed. Table 1 summarizes the RMS of the $\mu_{1/2}$-distributions for modules containing more than 30 hits in each subdetector before and after alignment compared to Monte-Carlo alignment and ideal Monte-Carlo. The coordinate u' is the most sensitive coordinate oriented along global r-ϕ, and v' is the second coordinate in the pixel system.

6.3. *Systematic effects*

Due to a weak or non-existing sensitivity of the given track sample to certain correlated deformation modes of the tracker, the absolute position of the modules in the tracker is less well known than the RMS of the $\mu_{1/2}$-distribution. Therefore, systematic deformations motivated by the cylindrical tracker structure have been introduced to the geometry and the alignment procedure has been re-run. This way the sensitivity of the track sample to the deformation under study can be evaluated. Figure 7 illustrates the alignment of a tracker where a systematic layer rotation has been introduced in the TIB and TOB. Before this distortion, $r\Delta\phi$ is equal to zero for all modules. Then modules are repositioned according to the parabolic (black) line. This deformation increases the χ^2 of tracks. Aligning

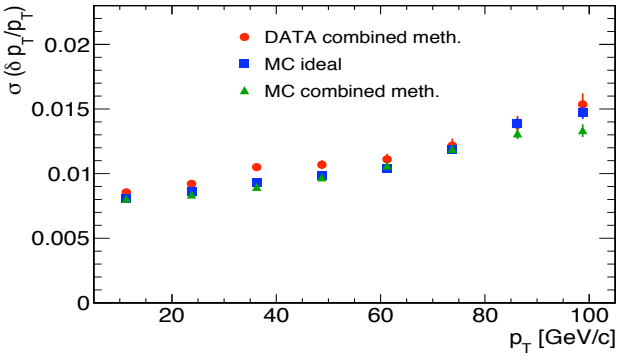

Figure 8: Momentum resolution obtained from split tracks as function of p_T.

the tracker, the χ^2 can be restored to the value before the deformation. The modules are moved into new, "aligned" positions. However, there is a remaining distortion of the modules, as the vertical (red) bands indicate in Figure 7. Other systematic deformations also have been studied [5].

7. Tracking performance

Tracking performance has been evaluated after alignment. Tracks were split at the distance of closest approach (DCA) to the beam line, and each part was required to have at least three pixel hits, mimicking collision tracks. Both track parts then were refitted individually, and the track parameters were evaluated at the DCA. As an example, Figure 8 shows the RMS of the distribution of the differences of $1/p_T$ for the two track parts as a function of p_T scaled by $1/\sqrt{2}$ to account for the two independent measurements. Results for the other track parameters are given in Reference [5].

8. Summary

The CMS tracker performance after calibration and alignment with cosmic muon and collision data is excellent. A signal-to-noise ratio of 26–32 is obtained. The Lorentz angle has been measured, and dE/dx measurements separate kaons from protons. High hit- and tracking efficiency and close to ideal track parameters are obtained after alignment.

References

[1] CMS Collaboration, "The CMS experiment at the CERN LHC", 2008 JINST **3** S08004. doi:10.1088/1748-0221/3/08/S08004.

[2] M. Raymond et al., "The CMS Tracker APV 25 0.25 μm CMOS readout chip", in Proceedings of the 6th Workshop on Electronics for LHC Experiments, Cracow Poland (2000).

[3] CMS Collaboration, "Commissioning and Performance of the CMS Silicon Strip Tracker with Cosmic Ray Muons ", 2010 JINST **5** T03008. doi: 10.1088/1748-0221/5/03/T03008

[4] W. Adam et al., "Stand-alone Cosmic Muon Reconstruction Before Installation of the CMS Silicon Strip Tracker", 2009 JINST **4** P05004. doi:10.1088/1748-0221/4/05/P05004.

[5] CMS Collaboration, "Alignment of the CMS Silicon Tracker during Commissioning with Cosmic Rays", 2010 JINST **5** T03009. doi: 10.1088/1748-0221/5/03/T03009